Predicting the Phase Equilibria of Mixtures of Hydrogen Fluoride with Water, Difluoromethane (HFC-32), and 1,1,1,2-Tetrafluoroethane (HFC-134a) Using a Simplified SAFT Approach

Amparo Galindo, Paul J. Whitehead, and George Jackson*

Department of Chemistry, University of Sheffield, Sheffield, S3 7HF, UK

Andrew N. Burgess

Research and Technology, ICI Chemicals and Polymers, PO Box 8, The Heath, Runcorn, Cheshire, WA7 4QD, UK

Received: August 30, 1996[⊗]

A simplified version of the statistical associating fluid theory (SAFT) is used to describe the thermodynamic properties and hence predict the phase equilibrium in associating mixtures containing hydrogen fluoride (HF). In the SAFT-HS approach the molecules are treated as hard spheres or chains of hard spherical segments with square-well association sites to mediate the hydrogen-bonding interactions and with van der Waals dispersion forces treated at the mean field level. Hydrogen fluoride is represented by a two association site model, as are the refrigerant molecules difluoromethane (HFC-32) and 1,1,1,2-tetrafluoroethane (HFC-134a), while water (H_2O) is represented by a four-site model. The intermolecular parameters of the pure components are determined in order to give the best representation of the vapor pressures and saturated liquid densities. The unlike intermolecular parameters of the mixtures are adjusted to specific features of the system: in the case of the H_2O + HF system the azeotropic temperature at atmospheric pressure is used, while for the HFC-32 + HF and HFC-134a + HF systems bubble-point compositions are used. The SAFT-HS approach provides an excellent representation of the H_2O + HF mixture over a large temperature and pressure range. The predicted phase equilibria of hydrogen fluoride mixtures with refrigerants are also in good agreement with experimental data; the presence of liquid−liquid equilibria in the mixture of HFC-134a + HF is predicted by the theory. It is hoped that the SAFT approach will be used as a predictive tool to describe these systems which are of importance in the manufacture of replacement refrigerants.

1. Introduction

The development of fluorocarbon chemistry dates back to the turn of the century when Swarts[1] described a reaction that, starting from tetrachloromethane (CCl_4) and hydrogen fluoride (HF), yielded a wide variety of chlorofluorocarbons (CFCs). These systems are in widespread use in many areas of modern society, as refrigerants, foam-blowing agents, industrial solvents, and cleaning agents. By the mid-1980s, however, it was confirmed that CFCs were responsible for the depletion of the ozone layer over Antarctica. In 1987 most industrialized countries signed the Montreal Protocol calling for a 50% reduction of the CFC production by 1998; in a later review the total phasing out of CFCs by 1995, and of hydrochlorofluorocarbons (HCFCs) by 2030, was agreed. Hydrofluorocarbons (HFCs), e.g., difluoromethane (HFC-32) and 1,1,1,2-tetrafluoroethane (HFC-134a), are now being manufactured as ozone-friendly replacements, although mixtures of HFCs, rather than pure substances, prove more suitable.

The first quantitative description of HF vapor was given by Simons and Hildebrand:[2] they showed that their measurements of the density of HF vapor, and those of Thorpe and Hambly,[3] could be reproduced in terms of two molecular species, a monomer and a hexamer. Fredenhagen[4] obtained new data for the vapor densities and concluded that longer polymer aggregates should exist at high pressures, with smaller aggregates at lower pressures. The association of gaseous HF was again studied by Long et al.,[5] who obtained fair agreement with the data of Simons and Hildebrand[2] and also discussed the presence of lower polymeric aggregates. Jarry and Davis[6] observed that the logarithm of the vapor pressure of HF as a function of the inverse of the temperature (Clausius−Clapeyron curve) is concave upward, the opposite of what is normally found; this feature was explained in terms of association. We will see later that this anomalous behavior can be reproduced with an extended SAFT treatment. The possibility of explicitly accounting for association in the vapor phase of HF systems was examined by Armitage et al.[7] Association in the gas was also treated by Redington,[8,9] who calculated the second virial coefficients and oligomer properties using six different potentials for the HF−HF interaction and presented a nonideal continuous association model for temperatures between 19.5 and 56 °C (292.5−329 K). Reviews of work on the HF system up to the late 1950s can be found in refs 10 and 11; much of the information on the thermodynamic properties up to 1970 is collected in ref 12.

The phase behavior of H_2O + HF mixtures was investigated in the 1940s with a principal focus on the recovery of fluorine from gases containing a small percentage of HF. The partial pressures of hydrogen fluoride and water vapor over aqueous solutions of hydrofluoric acid containing 2−30 wt % hydrogen fluoride were determined by Brosheer et al.[13] using a dynamic method from 25 to 75 °C (298−348 K); correlations of the data with empirical equations were also reported. In the same year, Munter et al.[14] measured the vapor−liquid equilibrium data of H_2O + HF at atmospheric pressure (0.101 325 MPa) and found an azeotrope with a composition of 38.26 wt % HF (mole

[⊗] Abstract published in *Advance ACS Abstracts,* January 15, 1997.

S1089-5647(96)02675-2 CCC: $14.00

fraction of $x = 0.358$) and a maximum boiling temperature of 112 °C (385 K). The occurrence of this extreme negative azeotropy provides an indication of the large nonideality of the system, in which the unlike attractive forces are considerably stronger than for the separate pure components. These authors later presented more experimental vapor pressure data measured with a dynamic technique for 10−70% hydrofluoric acid solutions at temperatures from 0 to 70 °C (273−343 K);[15] the pressure of the mixture is somewhat lower than the values calculated by Brosheer et al.[13] for the 10 and 20% solutions and in good agreement for the 30% solution. More recently, Miki et al.[16] developed a conductivity method to determine the phase equilibria of a mixture of water and hydrogen fluoride for systems with trace amounts of water and obtained a wider region of gas−liquid coexistence than the one described by Munter and co-workers.[14,15]

As well as being a central component in the transformation of CFCs into HFCs,[17] hydrogen fluoride is one of the most extensively studied hydrogen-bonded materials. This particular interest in HF is a consequence of its small size and the strength of the hydrogen-bond in the solid, liquid, and gaseous phases. In crystalline HF the molecules form infinite chains of hydrogen bonded HF monomers.[18] A similar type of aggregation is expected in the liquid phase,[19] and oligomers of HF are well-known to be present in the gas phase below about 80 °C (353 K).[6,9,11,20−24] The hexamer is commonly believed to be the most prevalent aggregate in the gas phase although its abundance and that of the other aggregates ranging from the dimer to the nonamer is not clear. The HF dimer corresponds to a bent chain[23] and the hexamer to a cyclic (ring) structure;[9,24] the latter was suggested very early on by Simons and Hildebrand.[2] *Ab initio* calculations of small clusters of HF have been undertaken in a number of studies.[25−29] One of the most interesting recent studies of the aggregation in gaseous HF is the Monte Carlo simulations study by Zhang et al.[30] using the central force potential developed by Klein and McDonald.[31] Extensive simulation studies of the liquid phase of HF with both Monte Carlo and molecular dynamic techniques have also been reported (e.g., see refs 32−36). There is some disagreement about the shape of the first peak of the radial distribution for the different potentials, but in all cases chainlike aggregated structures of hydrogen-bonded monomers, similar to the ones found in the solid,[18] are found.

The industry of replacement refrigerants has renewed the interest in HF and in its mixtures with other fluorinated agents and with water. Central to this is the development of an accurate equation of state (EOS) for the description of the thermodynamic properties and phase equilibria of HF systems. The problem of association in HF was initially addressed by the separate solution of two different models: while the gas is described in terms of a chemical equilibrium of monomers and hexamers, the liquid is assumed not to exhibit association.[37,38] Other approaches involve cubic equations of state, such as the Peng−Robinson EOS, with modifications to describe association: Twu et al.[39] described the thermodynamic properties of HF using a monomer−hexamer model where the equilibrium constant is taken from the data of Long et al.,[5] and Chai Kao et al.[40] used a very similar EOS to correlate data for 21 pure compounds, including halogenated compounds, hydrogen fluoride, and water. A cubic EOS with separate contributions for the chemical and physical contributions has also been used to study HF[41,42] and mixtures of HF with other halocarbons.[43] An infinite model for association is used to describe the chemical association, and the distribution of oligomers in HF is assumed to be a Poisson-like function. More recently, Economou and Peters[44] have studied HF and mixtures of HF with halocarbons using the associated perturbed anisotropic chain theory (APACT) with an equilibrium model that includes monomers, dimers, trimers, hexamers, and nonamers. They find good agreement with experimental data for the vapor−liquid equilibrium of different mixtures and observe liquid−liquid immiscibility at low temperatures, a feature of the phase behavior that has not yet been confirmed experimentally.

The statistical associating fluid theory (SAFT),[45−48] which is based on the work of Wertheim,[49−52] provides an alternative approach to describe associated systems. The main advantage of using SAFT rather than a chemical approach is that the chemical equilibria involved and their temperature and density dependence do not have to be specified explicitly. The SAFT EOS offers a molecular theory with a firm foundation in statistical mechanics where the association is treated at the level of anisotropic intermolecular interactions. In a recent paper,[53] we have reviewed the main developments and applications of SAFT, from simple spherical molecules to complex systems such as polymers. The SAFT EOS is one of the most accurate and successful EOS for the prediction of phase equilibria. In this paper we apply the EOS to HF systems. The theory of Wertheim has now been extended to deal with intramolecular association,[54−57] including ring formation, and hydrogen bond cooperativity,[58] a phenomenon that is also observed in $(HF)_3$.[59] These studies present a theoretical framework for an accurate description of HF that could include the finer experimental features of the system. However, in the present work we use a simpler version of SAFT, which we called SAFT-HS,[53,60,61] to study HF and three HF mixtures: H_2O + HF, HFC-32 + HF, and HFC-134a + HF. We have chosen a two-site model for HF that allows the formation of chains of hydrogen-bonded monomers but have not treated the effect of ring formation. It turns out that this simple model provides a very good description of the phase equilibria of these mixtures. The effect of ring formation in HF systems will be examined in future work.

2. Models and Theory

Because of the numerous versions of SAFT in the literature, we summarize the details of our simplified SAFT-HS[53,60,61] approach before comparing our results with experimental data. The molecules are modeled as hard spherical repulsive cores formed from tangentially bonded segments of diameter σ with a number of embedded off-center square-well bonding sites. The association sites are placed at a distance r_d from the center of the sphere and have a cutoff range r_c; these two parameters define the so-called bonding volume K.[60] When two sites are a distance of less than r_c apart, there is a site−site attractive interaction ϵ^{hb}. In SAFT-HS the long-range dispersion forces are included at the mean-field level of van der Waals, where the integrated energy of the mean-field attraction is described by a van der Waals attractive parameter α. In water four bonding sites are included on a central hard-sphere core; two sites account for the oxygen lone pairs and two for the hydrogens, and only oxygen−hydrogen site−site interactions are allowed. The sites can be viewed as placed in tetrahedral fashion (see Figure 1a), although at this level of approximation (the first-order theory of Wertheim) the precise geometry is not important. A similar four-association-site model for water was also proposed by Nezbeda and co-workers[62−64] and has already been used in studies of the phase equilibria of aqueous solutions.[65−69,53] It is important to note that Nezbeda and co-workers call this a five-site model for water, counting the hard core as a central site. We model hydrogen fluoride as a central

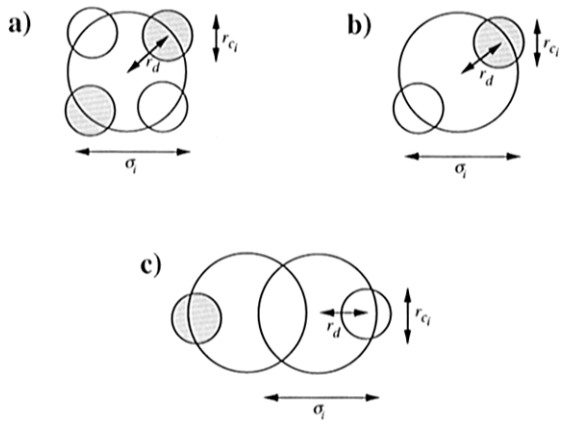

Figure 1. Models for (a) H_2O, (b) HFC-32 and HF, and (c) HFC-134a. A number of off-center square-well bonding sites are placed on a hard sphere of diameter σ_i. The sites are at a distance $r_d^* = 0.25$ from the center of the sphere and have a range r_c^*. The two different types of sites are colored white and gray; only white−gray bonding is allowed. The white and black sites interact with a hydrogen-bonding energy ϵ^{hb} when the site−site distance is less than r_c^*. H_2O, HFC-32, and HF are modeled with a single hard sphere ($m = 1$), while HFC-134a is modeled with $m = 1.35$ spheres (see text). A mean-field dispersive interaction is included per spherical segment with an integrated energy ϵ.

hard-sphere core with two attractive sites *a* and *b*, with, say, a bond angle of 180° (Figure 1b); again, the geometry is not important at this level of approximation. Only *a*−*b* bonding is allowed in this model, which allows it to form chain and ring aggregates of hydrogen-bonded monomers (although the latter are not treated at this level of approximation), but not treelike structures. In this, our first study on HF, we have chosen the simplest possible model within the SAFT framework; it turns out to be a good approximation. Better agreement with experimental data would be obtained if the more sophisticated versions of SAFT were used and if ring formation was accounted for in the theory. Both HFC-32 and HFC-134a are polar molecules, but it is not clear whether or not they hydrogen bond. Recent experimental neutron scattering data for trifluoromethane (HFC-24) suggest that these molecules do not form hydrogen bonds.[70] Our models for these refrigerants do not include an explicit contribution for the polar interactions, but include two bonding sites (as for HF) in the hope of modeling the dipolar anisotropy of the system; we treat the attractive interaction due to the dipoles, or weak hydrogen bonds, as a type of association. The hard repulsive core of HFC-32 is modeled with a single hard sphere (Figure 1b), while $m = 1.35$ spheres, two fused hard spheres, are used for HFC-134a (Figure 1c). The parameter *m* in the SAFT approach accounts for the number of spherical segments in the chain and essentially describes the asymmetry in the molecular shape (e.g., see the work by Boublík[71] for the relationship between *m* and the nonsphericity of the molecule). This parameter is, to some extent, fitted to give the best agreement with experimental data, although it is important to retain a physically reasonable molecular shape.

In order to describe the phase equilibria of the real systems, the calculated vapor pressures and saturated liquid densities are fitted to experimental data (from the triple point to the critical point for the pure substances) to determine the optimum set of parameters for the models. In this way we obtain values for the size of the hard sphere σ, the strength of the mean-field interaction ϵ^{mf}, the range of the cutoff distance for the site−site interaction r_c, and the strength of the site−site hydrogen-bonding interaction ϵ^{hb}. The sites are always placed at a distance $r_d/\sigma = 0.25$ from the central sphere, so that the bonding volume *K* is determined once r_c is set.[60] Before discussing the result of the fits to the experimental data, it is convenient to briefly review the theoretical expressions of SAFT-HS as it is a simplified version of the original SAFT approach.[45−48] The reader should also refer to the original papers[60,61] for a more detailed description of the SAFT-HS theory.

Here, we follow the same approach as in our previous paper;[53] we first give the general theory and then the specific expressions for our mixtures. The Helmholtz free energy *A* for an *n*-component mixture of associated spherical molecules is separated into different contributions as

$$\frac{A}{NkT} = \frac{A^{ideal}}{NkT} + \frac{A^{hs}}{NkT} + \frac{A^{chain}}{NkT} + \frac{A^{assoc}}{NkT} + \frac{A^{mf}}{NkT} \quad (1)$$

where *N* is the number of molecules, *T* is the temperature, and *k* is the Boltzmann constant The ideal contribution to the free energy is given by[72]

$$\frac{A^{ideal}}{NkT} = \left(\sum_{i=1}^{n} x_i \ln \rho_i \Lambda_i^3\right) - 1 = x_1 \ln \rho_1 \Lambda_1^3 + x_2 \ln \rho_2 \Lambda_2^3 - 1 \quad (2)$$

The sum is over all species *i* of the mixture; $x_i = N_i/N$ is the mole fraction, $\rho_i = N_i/V$ the number density, N_i the number of molecules, Λ_i the thermal de Broglie wavelength of species *i*, and *V* the volume of the system. The expression of Boublík[73] (equivalent to that of Mansoori et al.[74]) for a multicomponent mixture of hard spheres is used to account for the reference hard-sphere contribution, i.e.,

$$\frac{A^{hs}}{NkT} = \frac{6}{\pi\rho}\left[\left(\frac{\zeta_2^3}{\zeta_3^2} - \zeta_0\right)\ln(1-\zeta_3) + \frac{3\zeta_1\zeta_2}{1-\zeta_3} + \frac{\zeta_2^3}{\zeta_3(1-\zeta_3)^2}\right] \quad (3)$$

and the corresponding radial distribution function for a mixture of hard spheres with different diameters is

$$g^{hs}(\sigma_{ij}) = \frac{1}{1-\zeta_3} + 3\frac{\sigma_i\sigma_j}{\sigma_i+\sigma_j}\frac{\zeta_2}{(1-\zeta_3)^2} + 2\left(\frac{\sigma_i\sigma_j}{\sigma_i+\sigma_j}\right)^2\frac{\zeta_2^2}{(1-\zeta_3)^3} \quad (4)$$

In eq 3 $\rho = N/V$ is the total number density of the mixture, while the reduced densities ζ_l are defined as

$$\zeta_l = (\pi\rho/6)\left[\sum_{i=1}^{n} x_i m_i (\sigma_i)^l\right] = (\pi\rho/6)[x_1 m_1 (\sigma_1)^l + x_2 (\sigma_2)^l] \quad (5)$$

ζ_3 is the total packing fraction of the mixture, σ_i the diameter of component *i*, and m_i the number of spherical segments in a chain of component *i*. Note that component 2 is always HF with $m_2 = 1$; when component 1 is spherical as for H_2O or HFC-32 $m_1 = 1$, while for HFC-134a the best description of the phase equilibria is provided with $m_2 = 1.35$ (see later). The contribution to the free energy due to the formation of the chain molecule (HFC-134a) is[61]

$$\frac{A^{chain}}{NkT} = -\sum_{i=1}^{n} x_i (m_i - 1)\ln g^{hs}(\sigma_{ii}) \quad (6)$$

$$= -x_1 (m_1 - 1)\ln g^{hs}(\sigma_{11}) \quad (7)$$

where $m_1 = 1.35$ for mixtures with HFC-134a; for all other systems $A^{chain}/NkT = 0$. The contribution due to association for s_i sites on a molecule of species i is obtained from the theory of Wertheim (see ref 61) as

$$\frac{A^{assoc}}{NkT} = \sum_{i=1}^{n} x_i \left[\sum_{a=1}^{s_i} \left(\ln X_{a,i} - \frac{X_{a,i}}{2} \right) + \frac{s_i}{2} \right] \tag{8}$$

The first sum is over the species i, the second is over all s_i sites a on a molecule i, and $X_{a,i}$ is the fraction of molecules of type i not bonded at site a. For the mixture of H_2O (1) + HF (2) we can write eq 8 as

$$\frac{A^{assoc}}{NkT} = x_1 \left[4\left(\ln X_1 - \frac{X_1}{2} \right) + 2 \right] + x_2 \left[2\left(\ln X_2 - \frac{X_2}{2} \right) + 1 \right] \tag{9}$$

As far as the fractions of molecules not bonded are concerned, all of the sites in a molecule of a certain type i are equivalent, so that H_2O has four equivalent contributions and HF has two. X_1 is the fraction of H_2O molecules not bonded at a given site, and X_2 is the fraction HF molecules not bonded at a given site. For the HFC (1) + HF (2) mixtures, the contribution to the free energy due to association is given by

$$\frac{A^{assoc}}{NkT} = x_1 \left[2\left(\ln X_1 - \frac{X_1}{2} \right) + 1 \right] + x_2 \left[2\left(\ln X_2 - \frac{X_2}{2} \right) + 1 \right] \tag{10}$$

since both components of the mixtures have two bonding sites. The fractions of molecules not bonded at a given site $X_{a,i}$ in eq 8 can be obtained by a self-consistent iterative solution of the mass action equation:[61]

$$X_{a,i} = \frac{1}{1 + \sum_{j=1}^{n} \sum_{b=1}^{s_j} \rho x_j X_{b,j} \Delta_{a,b,i,j}} \tag{11}$$

The function $\Delta_{a,b,i,j}$ characterizes the association between site a on a molecule of species i and site b on a molecule of species j. It can be written in terms of the contact value $g^{hs}(\sigma_{ij})$ of the radial distribution function of the reference segment−segment hard-sphere interaction (eq 4), the Mayer f function $f_{a,b,i,j} = \exp(-\phi_{a,b,i,j}/kT) - 1$ of the $a-b$ site−site bonding interaction $\phi_{a,b,i,j}$, and the volume $K_{a,b,i,j}$ available for bonding:[61]

$$\Delta_{a,b,i,j} = K_{a,b,i,j} f_{a,b,i,j} g^{hs}(\sigma_{ij}) \tag{12}$$

Because in this case the bonding for the sites on a given type of molecule is equivalent, the subscripts for the type of site are dropped, and $\Delta_{a,b,i,j}$ becomes

$$\Delta_{ij} = K_{ij} F_{ij} g^{hs}(\sigma_{ij}) \tag{13}$$

where

$$F_{ij} = \exp(-\epsilon_{ij}^{hb}/kT) - 1 \tag{14}$$

and i and j refer to component 1 or 2, not to the type of site; the site−site interaction ϵ_{ij}^{hb} is assumed to be of the square-well type. For a mixture of H_2O (component 1) and HF (component 2),

$$X_1 = \frac{1}{1 + 2\rho x_1 X_1 \Delta_{11} + \rho x_2 X_2 \Delta_{12}} \tag{15}$$

and

$$X_2 = \frac{1}{1 + 2\rho x_1 X_1 \Delta_{21} + \rho x_2 X_2 \Delta_{22}} \tag{16}$$

Note that the factor of 2 for the contribution due to water−water association (second term in the denominator of eq 15) was erroneously given as 4 in ref 53. The fractions of molecules not bonded at a given site for the HFC + HF mixtures are obtained from the following expressions:

$$X_1 = \frac{1}{1 + \rho x_1 X_1 \Delta_{11} + \rho x_2 X_2 \Delta_{12}} \tag{17}$$

and

$$X_2 = \frac{1}{1 + \rho x_1 X_1 \Delta_{21} + \rho x_2 X_2 \Delta_{22}} \tag{18}$$

It is important to note that the extent of association depends on the strength of the interaction via F and on the position and range of the site−site interaction via K. The precise details of the position and range of the sites are not important at this level of approximation so long as they correspond to the same integrated bonding volume. Finally, the contribution due to the dispersive attractive interactions is given at the mean-field level in terms of the van der Waals one-fluid theory of mixing for the segments:[53,72]

$$\frac{A^{mf}}{NkT} = -\frac{\rho}{kT} \sum_{i=1}^{n} \sum_{j=1}^{n} \alpha_{ij} x_i x_j m_i m_j = -\frac{\rho}{kT} (\alpha_{11} x_1^2 m_1^2 + 2\alpha_{12} x_1 x_2 m_1 + \alpha_{22} x_2^2) \tag{19}$$

where $m_1 = 1$ for the H_2O (1) + HF (2) and HFC-32 (1) + HF (2) systems, and $m_1 = 1.35$ for the HFC-134a (1) + HF (2) system. The α_{ij} are the van der Waals constants for the interactions between segments i and j.

The other thermodynamical properties can be obtained from the Helmholtz free energy using the standard relationships. The chemical potential of species i is given by

$$\mu_i = \left(\frac{\partial A}{\partial N_i} \right)_{T,V,N_{j \neq i}} \tag{20}$$

and the compressibility factor by

$$Z = \frac{pV}{NkT} = \sum_{i}^{n} \left(x_i \frac{\mu_i}{kT} \right) - \frac{A}{NkT} \tag{21}$$

These functions are required for the determination of the critical lines and phase behavior of the mixture. The gas−liquid and liquid−liquid critical lines can be determined by equating the second and third derivatives of the Gibbs free energy with respect to the mole fraction to zero, and phase equilibria between phases I and II in mixtures require that the temperature, pressure, and chemical potential of each component in each phase are equal,[72,75] i.e.,

$$T^{I} = T^{II}, \quad p^{I} = p^{II}, \quad \mu_i^{I} = \mu_i^{II} \tag{22}$$

These conditions for phase equilibria are solved numerically using a simplex method.[76] At this point it is convenient to define a number of reduced parameters that are useful in the

TABLE 1: Optimized Parameters for the Models of Water (H_2O), Hydrogen Fluoride (HF), Difluoromethane (HFC-32), and 1,1,1,2-Tetrafluoroethane (HFC-134a)[a]

	m	σ/Å	(ϵ/k)/K	(ϵ^{hb}/k)/K	K/Å^3	r_c^*	T_c^*	p_c^*
H_2O	1	3.596	4452	1558	1.3578	0.679	0.147 590	0.008 814 56
HFC-32	1	3.705	2207	1426	5.2028	0.765	0.165 934	0.006 442 22
HFC-134a	1.35	4.020	2373	1487	4.2162	0.730	0.163 427	0.005 124 01
HF	1	3.692	2451	2125	6.6580	0.787	0.193 846	0.005 647 48

[a] m is the number of spherical segments in the model, σ the diameter of each hard-sphere segment, ϵ the integrated mean-field energy per spherical segment, ϵ^{hb} the energy of the site−site hydrogen bond, K the bonding volume for the site−site interaction, and r_c^* the cutoff range corresponding to each K. T_c^* and p_c^* are the theoretical critical points in reduced units.

calculations. The volume of a spherical segment is denoted by $b_{ij} = \pi\sigma_{ij}^3/6$ (where $\sigma_{ij} = (\sigma_i + \sigma_j)/2$), and the integrated energy of the van der Waals mean-field interaction $\epsilon_{ij} = \alpha_{ij}/b_{ij}$. In a mixture all the parameters are reduced relative to one of the components, component 1 in our case, so that $\sigma_{ij}^* = \sigma_{ij}/\sigma_1$, $\alpha_{ij}^* = \alpha_{ij}/\alpha_{11}$, etc. The range and position of the bonding sites are reduced with respect to the diameter of the particular sphere in which they are included, i.e., $r_{c1}^* = r_{c1}/\sigma_1$ and $r_{d1}^* = r_{d1}/\sigma_1$ while $r_{c2}^* = r_{c2}/\sigma_2$ and $r_{d2}^* = r_{d2}/\sigma_2$. The reduced bonding volume for each of the pure components is calculated as

$$K_{ii}^* = K_{ii}/\sigma_i^3 = 4\pi\{\ln(r_c^* + 2r_d^*)(6r_c^{*3} + 18r_c^{*2}r_d^* - 24r_d^{*3}) + (r_c^* + 2r_d^* - 1)(22r_d^{*2} - 5r_c^*r_d^* - 7r_d^* - 8r_c^{*2} + r_c^* + 1)\}/72r_d^{*2} \quad (23)$$

and can then be written in terms of one of the two components. The reduced energy for the site−site interaction is defined in terms of the mean-field interaction of component 1, $\epsilon_{ij}^{hb*} = \epsilon_{ij}^{hb}/\epsilon_1$. The reduced dimensionless temperatures and pressures are defined as $T^* = kTb/\alpha = kT/\epsilon$ and $p^* = pb^2/\alpha = pb/\epsilon$, where the subscript c is sometimes used to denote the critical point.

3. Results

Before studying the mixtures, the parameters of the potential models for the pure substances have to be determined by fitting the theoretical predictions to the experimental phase equilibria using a simplex method.[76] The optimized values for the diameter of the hard core σ/Å, the strength of the mean-field interaction ϵ/k, the strength of the association site−site energy ϵ^{hb}/K, the bonding volume K/Å^3 (with the corresponding r_c^*), and the chain length m for the pure substances are shown in Table 1; H_2O, HF, and HFC-32 are all treated as spherical with a fixed $m = 1$ while the value for the less spherical HFC-134a is optimized. It is important to note that the dispersion energies are larger than the hydrogen-bonding energies because the latter correspond to integrated values (like the van der Waals constant) and not to well depths.

In the optimization of the properties of pure HF only the experimental vapor pressures[10,12] were considered, but as we shall see the theoretical predictions of the properties of the phase equilibria of the mixtures are still very accurate. We find that a significantly better description of the vapor pressures is obtained if the densities are not considered in the determination of the parameters for the model. This is adequate because our comparisons with experimental data for the mixtures involve vapor-pressure data but no density data. In Figure 2 we show the vapor-pressure curve as a pT representation (Figure 2a) and as a Clausius−Clapeyron plot (Figure 2b), where the low-temperature behavior is clearly seen. The simple theory provides a good representation of the vapor-pressure curve of HF. The anomalous curvature of the vapor-pressure curve for HF is clearly observed in the experimental data at low temperatures (see Figure 2b). This anomaly can be explained

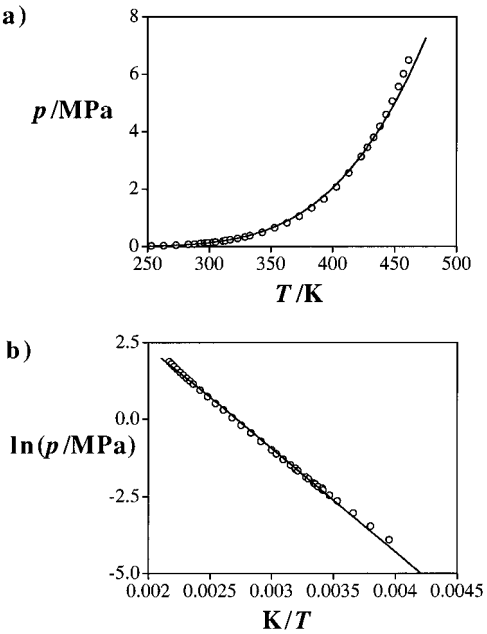

Figure 2. Vapor pressures for HF compared with the SAFT-HS predictions. The circles represent the experimental data.[10,12] The results obtained with the parameters (see Table 1) fitted to the experimental data are shown as continuous curves. In (a) we show the vapor-pressure curve as a pT representation and in (b) as a Clausius−Clapeyron plot.

in terms of ring formation in the vapor phase, which we have not treated in our simplified approach, so that the curvature is not reproduced. It is possible to account for ring formation within the formalism of Wertheim, and it has been shown that if ring formation is accounted for in a SAFT-like EOS, the anomalous upward curvature of the Clausius−Clapeyron plot is obtained.[56]

The water−water hydrogen-bond parameter is obtained by fitting to experimental vapor pressures and saturated liquid densities from the triple point to the critical point,[77] while the size parameter σ and the integrated mean-field energy ϵ are adjusted considering only the vapor pressures; the actual values are given in Table 1. A better agreement for the vapor-pressure curve and the critical region for water is obtained in this way. One should note that, unlike in our previous publication,[53] we do not scale the parameters to the critical point. The predicted vapor pressure of water is in good agreement with the experimental values (see Figure 3).

Both experimental vapor pressures and liquid densities[78] are used in the determination of all of the model parameters for HFC-32 and HFC-134a. Since we do not account for the dipolar interactions explicitly, it is important to ensure that the optimized parameters were consistent for a wide range of properties. The very good description of phase behavior up to the experimental critical points can be seen in Figures 4 and 5, with a slight overprediction of the experimental critical point. The description of dispersion forces at the mean-field level is partly responsible for this, although any analytical EOS will result in

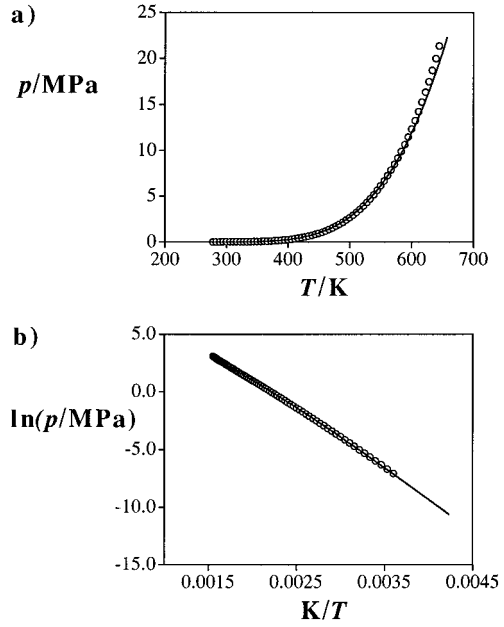

Figure 3. Vapor pressures for H_2O compared with the SAFT-HS predictions. The circles represent the experimental data.[77] The results obtained with the parameters (see Table 1) fitted to the experimental data are shown as continuous curves. In (a) we show the vapor-pressure curve as a *pT* representation and in (b) as a Clausius−Clapeyron plot.

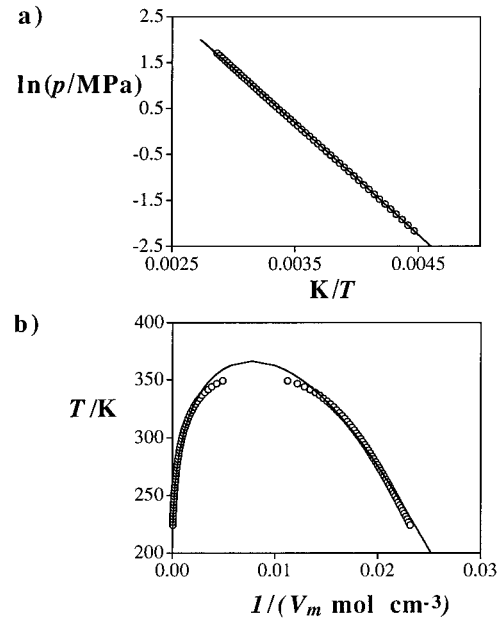

Figure 4. Vapor pressures and vapor−liquid coexistence densities for HFC-32 compared with the SAFT-HS predictions. The circles represent the experimental data.[78] The results obtained with the parameters (see Table 1) fitted to both experimental vapor pressures and saturated liquid densities are shown as continuous curves. In (a) we show the Clausius−Clapeyron plot of the vapor-pressure curve and in (b) the coexisting vapor and liquid densities.

a quadratic coexistence curve close to the critical point (classical critical behavior) instead of the near-cubic curve (universal critical behavior) observed experimentally.

The study of phase equilibria in mixtures also requires the determination of a number of so-called unlike parameters. The geometric mean is generally used to calculate the unlike energy parameters and the arithmetic mean to determine size-related parameters. Since our models comprise hard-sphere segments, the unlike size parameter σ_{12} is obtained as the arithmetic mean.

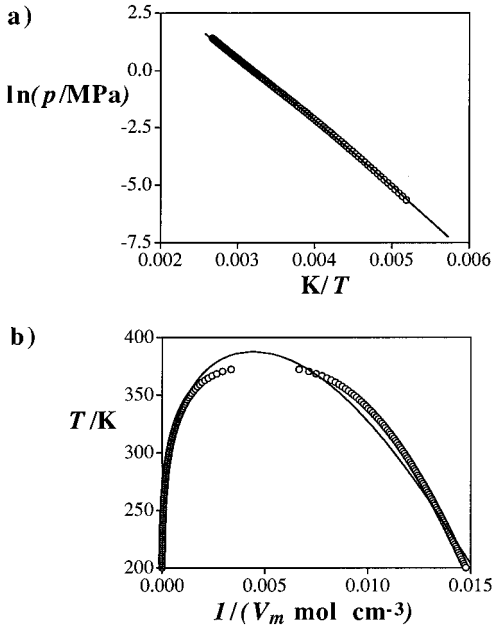

Figure 5. Vapor pressures and vapor−liquid coexistence densities for HFC-134a compared with the SAFT-HS predictions. The circles represent the experimental data.[78] The results obtained with the parameters (see Table 1) fitted to both experimental vapor pressures and saturated liquid densities are shown as continuous curves. In (a) we show the Clausius−Clapeyron plot of the vapor-pressure curve and in (b) the coexisting vapor and liquid densities.

Similarly, the bonding volume between sites on different molecules can be calculated as

$$K_{12}^{*} = \frac{K_{12}}{\sigma_1^{\,3}} = \left[\frac{(K_{11}/\sigma_1^{\,3})^{1/3} + (K_{22}/\sigma_1^{\,3})^{1/3}}{2}\right]^3 \qquad (24)$$

and is not readjusted. Some of the extreme features in the phase behavior of the mixtures considered in this study cannot be predicted with unlike energies calculated with the geometric mean. We treat the the unlike integrated mean-field energy ϵ_{12} and the site−site energy of the hydrogen bond between unlike molecules ϵ_{12}^{hb} as adjustable parameters and have optimized them to give the best representation of the properties of the mixtures, usually at one state point. With this single procedure we can then calculate the phase equilibria of the mixtures over an extensive range of temperatures and pressures.

A *Tx* slice at constant atmospheric pressure (0.101 325 MPa) for a mixture of H_2O (1) + HF (2) is shown in Figure 6. The parameters of the unlike interactions were obtained by fitting the theoretical predictions to the temperature and composition of the azeotrope at this pressure (T = 385 K, x_2 = 0.358). In this case the optimum values are ϵ_{12}/k = 4578 K and ϵ_{12}^{hb}/k = 2311 K (with corresponding reduced parameters of α_{12}^{*} = 1.070, α_2^{*} = 0.596, and ϵ_{12}^{hb*} = 0.519); the unlike bonding volume is obtained from eq 24 as K_{12} = 3.337 Å^3 and is not optimized. We used the data of Munter et al.,[14] which is the most comprehensive set of data found for this system, for comparisons with the theoretical predictions. The agreement of the theoretical phase behavior with the experimental data is found to be very good over the entire composition range of the mixture, although the bubble point temperature of the liquid in HF-rich mixtures is slightly underpredicted by the theory. In order to establish the adequacy of our parameters for the mixture over a wider range of temperatures and pressures, we have studied the vapor−liquid equilibria at four constant temperatures, from 25 °C (298 K) to 75 °C (348 K). The corresponding *px* slices of our theoretical predictions together with the experimental

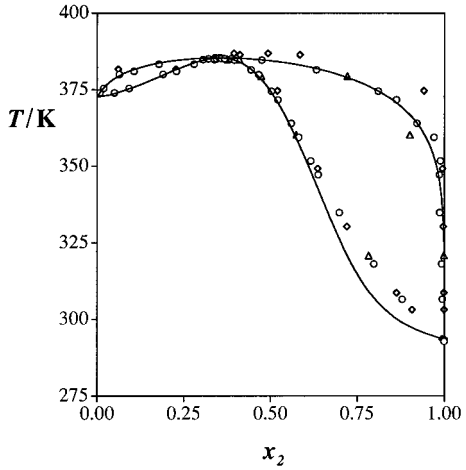

Figure 6. Constant pressure (0.101 325 MPa) *Tx* slice for a H_2O (1) + HF (2) mixture compared with the SAFT-HS predictions. The calculated coexisting compositions are shown as solid curves and the experimental data as symbols. The experimental data of Munter et al.[14] are represented as circles, that of Vieweg[79] as triangles, and that of Miki et al.[16] as diamonds. The intermolecular parameters were obtained by fitting the temperature and composition of the azeotrope: ϵ_{12}/k = 4578 K and ϵ_{12}^{hb*} = 0.519 for the unlike interaction. The pure component parameters are given in Table 1.

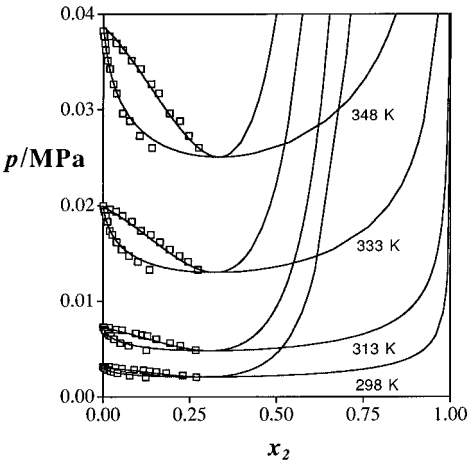

Figure 7. *px* slices at four constant temperatures for a mixture of H_2O (1) + HF (2) compared with the SAFT-HS predictions. The calculated coexisting compositions are shown as solid curves and the experimental data of Brosheer et al.[13] as squares. The values of the intermolecular parameters are given in Figure 6.

data[13] are shown in Figure 7. A very accurate prediction of the mixture properties is obtained with the values of the unlike parameters obtained at the higher pressure of 0.101 215 MPa and, more importantly, about 100 K higher in temperature. It is sometimes of more relevance in studies of distillation processes to examine the relation between the composition in the coexisting gaseous and liquid phases (*y* vs *x*); in this way it is possible to estimate the number of steps that are required in a distillation. We show the calculated and experimental compositions represented in this way in Figure 8 for a constant pressure slice of 0.101 215 MPa (Figure 8a) and for constant temperature slices of 298 and 348 K (Figure 8b). The agreement observed provides an indication of the adequacy of the SAFT-HS approach in describing the phase equilibria of this rather complex associating system.

The *pT* projection of the *pTx* surface for the mixture is given in Figure 9; the azeotropic line can be seen more clearly at low temperatures and pressures in the inset of the figure. The solid diamond indicates the pressure at which the unlike energy parameters were fitted. The mixture exhibits type I phase

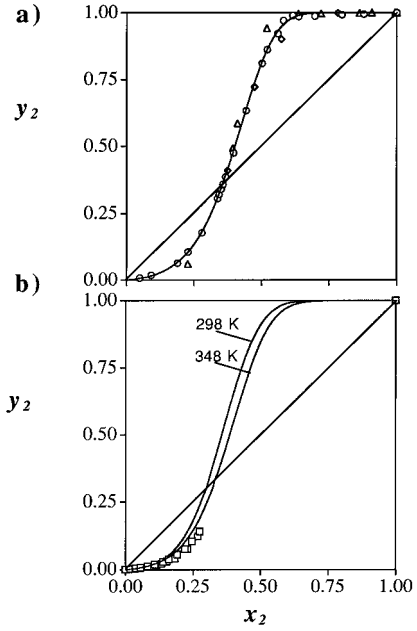

Figure 8. Mole fractions of HF (2) in the gaseous and liquid phases as a *xy* representation compared with experimental data. The experimental data are represented as symbols (see Figures 6 and 7 for references to the experimental data). The SAFT-HS predictions are shown as continuous curves. The compositions at constant atmospheric pressure (0.101 325 MPa) and at constant temperatures are shown in (a) and (b), respectively. The values of the intermolecular parameters are given in Figure 6.

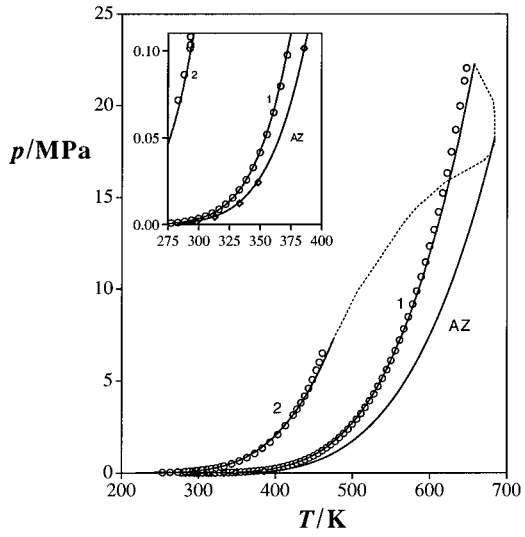

Figure 9. The *pT* projection for H_2O (1) + HF (2) compared with the SAFT-HS predictions. The experimental vapor pressures of H_2O[77] and HF[10,12] are shown as circles, and the experimental azeotropic points[13] are shown as diamonds. The calculated vapor pressures are plotted as continuous curves and labeled 1 and 2 for H_2O and HF, respectively, the continuous curve labeled AZ represents the calculated azeotropic curve, and the predicted gas−liquid critical line is represented as a dashed curve. The unlike interaction parameters (see Figure 6) were obtained by fitting the composition and temperature of the azeotrope at atmospheric pressure shown as a solid diamond.

behavior in the classification of Scott and van Konynenburg:[75] a continuous gas−liquid critical line extends from the critical point of HF to the critical point of H_2O, and the two components are miscible over the whole range. The predicted critical line exhibits an unusual shape: starting from the critical point of HF the gas−liquid critical line crosses over the vapor-pressure curve of pure H_2O and then merges into the azeotropic line at 683 K and 18.2 MPa before curving back to the critical point of H_2O. In Figure 10 we show the predicted *pTx* surface for

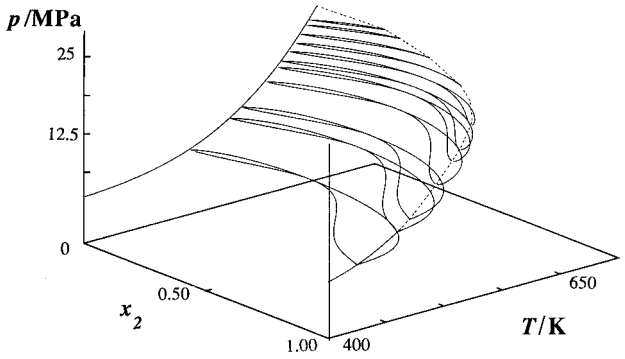

Figure 10. The *pTx* surface for H_2O (1) + HF (2). Constant-pressure *Tx* slices (continuous curves) and the gas−liquid critical line (dashed curve) are shown. The intermolecular parameters are given in Figure 6.

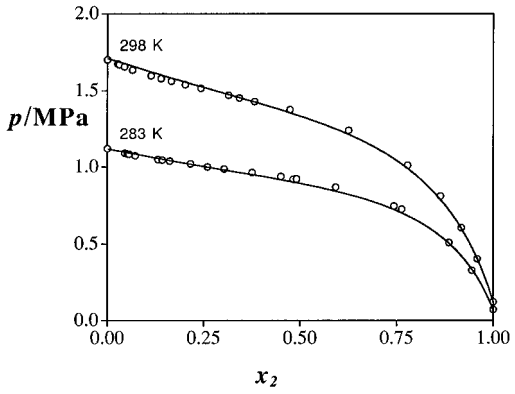

Figure 11. Bubble point pressures at constant temperature for a mixture of HFC-32 (1) + HF (2) compared with the SAFT-HS predictions. The experimental data are shown as circles.[80] The calculated bubble point pressures are shown as continuous curves. The unlike intermolecular parameters are $\epsilon_{12}/k = 2243$ K and $\epsilon_{12}^{hb*} = 0.655$. The pure component parameters are given in Table 1.

the mixture of H_2O (1) + HF (2). The disappearance of the azeotrope into the critical line can clearly be seen. The lack of experimental data in the high-pressure region for this highly corrosive mixture makes these predictions of particular interest.

To finish we present some predictions with the SAFT-HS approach for two mixtures of HF with replacement refrigerants: HFC-32 (1) + HF (2) and HFC-134a (1) + HF (2). The growing interest in the production of alternative refrigerants has resulted in a great deal of experimental data for these substances, only a fraction of which is for mixtures. We have focused our attention on ranges of pressure and temperature where the theoretical predictions can be compared with experimental measurements. The calculated bubble point pressures for a mixture of HFC-32 (1) + HF (2) at constant temperatures of 10 °C (283 K) and 25 °C (298 K) are compared with experimental data[80] in Figure 11. The unlike parameters in the mixture were optimized to give the best representation of the experimental data: the value of the unlike mean-field integrated energy is $\epsilon_{12}/k = 2243$ K, and that for the energy for the unlike site−site interaction is $\epsilon_{12}^{hb}/k = 1446$ K (with corresponding reduced parameters of $\alpha_{12}^{*} = 1.0113$, $\alpha_{22}^{*} = 1.099$, and $\epsilon_{12}^{hb*} = 0.655$). The bonding volume between two different sites is calculated from eq 24 as $K_{12} = 5.900$ Å^3 and is not readjusted. Our predictions suggest that this mixture exhibits type I phase behavior in the classification of Scott and van Konynenburg: the liquid region is fully miscible at all temperatures and pressures and a continuous gas−liquid critical line extends from the critical point of HFC-32 to the critical point of HF. The

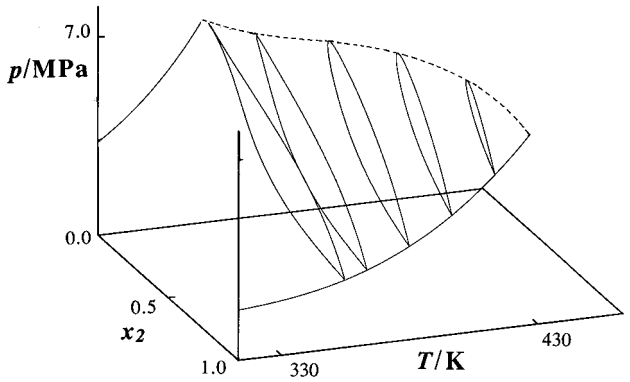

Figure 12. The *pTx* surface for HFC-32 (1) + HF (2). Constant temperature *px* slices (continuous curves) and the gas−liquid critical line (dashed curve) are shown. The intermolecular parameters are given in Figure 11.

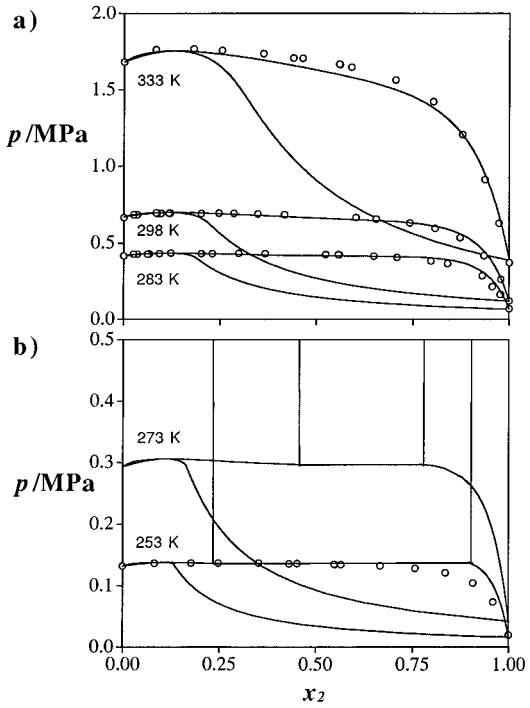

Figure 13. Bubble point pressures at constant temperature for a HFC-134a (1) + HF (2) mixture compared with the SAFT-HS predictions. The experimental bubble point pressures are shown as circles.[80,81] The calculated gas−liquid coexistence compositions are shown as continuous curves. Liquid−liquid coexistence is also predicted in (b). The values of the unlike intermolecular parameters are $\epsilon_{12}/k = 2195$ K and $\epsilon_{12}^{hb*} = 0.609$. The pure component parameters are given in Table 1.

corresponding *pTx* surface for HFC-32 (1) + HF (2) is shown in Figure 12.

The *px* slices for the HFC-134a (1) + HF (2) at temperatures of −20 °C (253 K), 0 °C (273 K), 10 °C (283 K), 25 °C (298 K), and 60 °C (333 K) determined with the SAFT-HS approach are compared with the experimental bubble point pressures[80,81] in Figure 13. The optimized unlike parameters of the mixture are $\epsilon_{12}/k = 2195$ K and $\epsilon_{12}^{hb}/k = 1446$ K (i.e., $\alpha_{12}^{*} = 0.816$, $\alpha_{22}^{*} = 0.800$, and $\epsilon_{12}^{hb*} = 0.609$), and the unlike bonding volume is $K_{12} = 5.344$ Å^3. As for the H_2O (1) + HF (2) system there is a positive azeotrope at low HF mole fractions (see Figure 13a). At low temperatures SAFT-HS predicts liquid−liquid phase separation as is shown in Figure 13b). Economou and Peters[44] have already suggested the presence of regions of liquid−liquid immiscibility for mixtures of HF with refrigerants, but this has not yet been confirmed experimentally. It is not surprising to observe liquid−liquid immiscibility when the

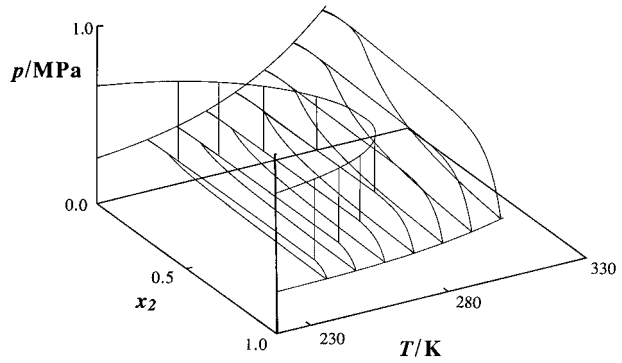

Figure 14. The *pTx* surface HFC-134a (1) + HF (2). Constant temperature *px* slices (continuous curves) are shown. The intermolecular parameters are given in Figure 13.

temperature is lowered in systems that exhibit positive azeotropy; weak unlike interactions are also the cause of positive azeotropy.[72] Finally, the *pTx* surface in the vicinity of the liquid−liquid immiscibility can be seen in Figure 14.

4. Conclusions

We hope to have demonstrated the suitability of even the simpler versions of SAFT to the prediction of the phase behavior of complex associating systems. The SAFT-HS approach provides an excellent quantitative representation of the phase equilibria of the H_2O + HF, HFC-32 + HF, and HFC-134a + HF systems which are of prime importance in the production of replacement refrigerants. The adequacy of the treatment suggests that the most important nonideal contribution in these mixtures is due to association so that the long-range dispersion forces can be treated at the rather crude van der Waals level. It is also clear that a two-site model can be used to study systems with strong dipole moments, removing the need to include a contribution for the dipolar interactions. Although this is not entirely satisfactory and a dipolar contribution should be incorporated in the theory, the treatment is reminiscent of the chemical approach in which one focuses on the aggregated species that are present in the system. Of course, the use of more sophisticated versions of SAFT is expected to improve the agreement with experiment. As was mentioned earlier, the formation of rings in the vapor phase of HF is an important factor in the low-temperature phase equilibria of HF systems. We plan to incorporate the extensions of the Wertheim theory for ring formation[56] into the SAFT expressions in order to study its effect on the phase behavior of these systems.

Acknowledgment. A.G. thanks Sheffield University and ICI Chemicals and Polymers Ltd. for the award of a Roberts-Boucher Scholarship, and P.J.W. thanks the ICI Strategic Research Fund for funding a Senior Research Fellowship. We also acknowledge support from the Royal Society (574005.G501/1992), from the European Commission (CI1*-CT94-0132), and from the Computational (GR/H58810-C91) and ROPA (GR/K34740) Initiatives of the EPSRC for computer hardware on which the calculations were performed.

References and Notes

(1) Swarts, F. *Bull. Acad. R. Belg.* **1892**, *24*, 309.
(2) Simons, J. H.; Hildebrand, J. A. *J. Am. Chem. Soc.* **1924**, *46*, 2183.
(3) Thorpe, T. E.; Hambly, F. J. *J. Chem. Soc.* **1889**, *55*, 163.
(4) Fredenhagen, K. *Z. Anorg. Allg. Chem.* **1934**, *218*, 161.
(5) Long, R. W.; Hildebrand, J. H.; Morrell, W. E. *J. Am. Chem. Soc.* **1943**, *65*, 182.
(6) Jarry, R. L.; Davis, W. J. *J. Phys. Chem.* **1953**, *57*, 600.
(7) Armitage, J. W.; Gray, P.; Wright, P. G. *J. Chem. Soc.* **1963**, 1796.
(8) Redington, R. L. *J. Chem. Phys.* **1981**, *75*, 4417.
(9) Redington, R. L. *J. Phys. Chem.* **1982**, *86*, 552.
(10) Frank, E. U.; Spalthoff, W. *Z. Electrochem.* **1957**, *61*, 348.
(11) Smith, D. F. *J. Chem. Phys.* **1958**, *28*, 1040.
(12) Vanderzee, C. E.; Rodenburg, W. W. M. *J. Chem. Thermodyn.* **1970**, *2*, 461.
(13) Brosheer, J. C.; Lenfesley, F. A.; Elmore, K. E. *Ind. Eng. Chem.* **1947**, *39*, 423.
(14) Munter, P. A.; Aepli, O. T.; Kossatz, R. A. *Ind. Eng. Chem.* **1947**, *39*, 427.
(15) Munter, P. A.; Otto, T. A.; Kossatz, R. A. *Ind. Eng. Chem.* **1949**, *41*, 1504.
(16) Miki, N.; Maneo, M.; Maruyashi, K.; Ohmi, T. *J. Electrochem. Soc.* **1990**, *137*, 787.
(17) Manzer, L. E. *Science* **1990**, *249*, 31.
(18) Cotton, F. A.; Wilkinson, G. *Advanced Inorganic Chemistry*, 5th ed. Wiley: New York, 1988.
(19) Sheft, I.; Perkins, A. J. *J. Inorg. Nucl. Chem.* **1976**, *38*, 665.
(20) Strochmeier, W.; Briegleb, G. *Z. Elektrochem.* **1953**, *57*, 662.
(21) Frank, E. U.; Meyer, F. *Z. Elektrochem.* **1959**, *63*, 571.
(22) Oriani, R. A.; Smyth, C. P. *J. Am. Chem. Soc.* **1948**, *70*, 125.
(23) Dyke, T. R.; Howard, B. J.; Klemperer, W. *J. Chem. Phys.* **1972**, *56*, 2442.
(24) Janzen, J.; Bartell, L. *J. Chem. Phys.* **1969**, *50*, 3611.
(25) Gaw, J. F.; Yamaguchi, Y.; Vincent, M. A.; Schaefer III, H. F. *J. Am. Chem. Soc.* **1984**, *106*, 3133.
(26) Scuseira, G. E.; Schaefer III, H. F. *Chem. Phys.* **1986**, *107*, 33.
(27) Karpfen, A.; Beyer, A.; Schuster, P. *Chem. Phys. Lett.* **1983**, *102*, 289.
(28) Liu, S.-Y.; Michael, D. W.; Dykstra, C. E.; Lisy, J. M. *J. Chem. Phys.* **1986**, *84*, 5032.
(29) Latajka, Z.; Scheiner, S. *Chem. Phys.* **1988**, *122*, 413.
(30) Zhang, C.; Freeman, D. L.; Doll, J. D. *J. Chem. Phys.* **1989**, *91*, 2489.
(31) Klein, M. L.; McDonald, I. R. *J. Chem. Phys.* **1979**, *71*, 298.
(32) Jorgensen, W. L. *J. Am. Chem. Soc.* **1978**, *100*, 7824.
(33) Jorgensen, W. L. *J. Chem. Phys.* **1979**, *70*, 5888.
(34) Cournoyer, M. E.; Jorgensen, W. L. *Mol. Phys.* **1984**, *51*, 119.
(35) Honda, K.; Kitaura, K.; Nishimoto, K. *Bull. Chem. Soc. Jpn.* **1992**, *65*, 3122.
(36) Laasonen, K.; Klein, M. L. *Mol. Phys.* **1996**, *88*, 135.
(37) Gillespie, P. C.; Cunningham, J. R.; Wilson, G. M. *AIChE Symp. Ser.* **1985**, *81* (244), 41.
(38) Schotte, W. *Ind. Eng. Chem. Process Des. Dev.* **1980**, *19*, 432.
(39) Twu, C. H.; Coon, J. E.; Cunningham, J. R. *Fluid Phase Equilib.* **1983**, *86*, 47.
(40) Chai Kao, C.-P.; Paulaitis, M. E.; Sweany, G. A.; Yokozeki, M. *Fluid Phase Equilib.* **1995**, *108*, 27.
(41) Anderko, A. *J. Chem. Soc., Faraday Trans.* **1990**, *86*, 2823.
(42) Anderko, A. *Fluid Phase Equilib.* **1991**, *65*, 89.
(43) Lenka, M.; Anderko, A. *AIChE J.* **1993**, *39*, 533.
(44) Economou, I. G.; Peters, C. J. *Ind. Eng. Chem. Res.* **1995**, *34*, 1868.
(45) Chapman, W. G.; Gubbins, K. E.; Jackson, G.; Radosz, M. *Fluid Phase Equilib.* **1989**, *52*, 31.
(46) Chapman, W. G.; Gubbins, K. E.; Jackson, G.; Radosz, M. *Ind. Eng. Chem. Res.* **1990**, *29*, 1709.
(47) Huang, S. H.; Radosz, M. *Ind. Eng. Chem. Res.* **1990**, *29*, 2284.
(48) Huang, S. H.; Radosz, M. *Ind. Eng. Chem. Res.* **1991**, *30*, 1994.
(49) Wertheim, M. S. *J. Stat. Phys.* **1984**, *35*, 19.
(50) Wertheim, M. S. *J. Stat. Phys.* **1984**, *35*, 35.
(51) Wertheim, M. S. *J. Stat. Phys.* **1986**, *42*, 459.
(52) Wertheim, M. S. *J. Stat. Phys.* **1986**, *42*, 477.
(53) Galindo, A.; Whitehead, P. J.; Jackson, G.; Burgess, A. N. *J. Phys. Chem.* **1996**, *100*, 6781.
(54) Ghonasgi, D.; Perez, V.; Chapman, W. G. *J. Chem. Phys.* **1994**, *101*, 6880.
(55) Ghonasgi, D.; Chapman, W. G. *J. Chem. Phys.* **1995**, *102*, 2585.
(56) Sear, R. P.; Jackson, G. *Phys. Rev. E* **1994**, *50*, 386.
(57) Sear, R. P.; Jackson, G. *Mol. Phys.* **1996**, *87*, 517.
(58) Sear, R. P.; Jackson, G. *J. Chem. Phys.* **1996**, *105*, 1113.
(59) Maes, G.; Smets, J. *J. Phys. Chem.* **1993**, *97*, 1818.
(60) Jackson, G.; Chapman, W. G.; Gubbins, K. E. *Mol. Phys.* **1988**, *65*, 1.
(61) Chapman, W. G.; Jackson, G.; Gubbins, K. E. *Mol. Phys.* **1988**, *65*, 1057.
(62) Nezbeda, I.; Kolafa J.; Kalyuzunyi, Y. V. *Mol. Phys.* **1989**, *68*, 143.
(63) Nezbeda, I.; Iglesias-Silva, G. A. *Mol. Phys.* **1990**, *69*, 767.
(64) Nezbeda, I.; Slovak, J. *Mol. Phys.* **1997**, *90*, 353.
(65) Green, D. G.; Jackson, G. *J. Chem. Soc., Faraday. Trans.* **1992**, *88*, 1395.
(66) Green, D. G.; Jackson, G. *J. Chem. Phys.* **1992**, *97*, 8672.
(67) Nezbeda, I.; Smith, W. R.; Kolafa, J. *J. Chem. Phys.* **1994**, *100*, 2191.
(68) Nezbeda, I.; Kolafa, J.; Pavlicek, J.; Smith, W. R. *J. Chem. Phys.* **1995**, *102*, 9638.

(69) Nezbeda, I.; Kolafa, J.; Smith, W. R. *Fluid Phase Equilib.*, submitted.

(70) Mort, K. A.; Johnson, K. A.; Cooper, D. L.; Burgess, A. N.; Howells, W. S. *Mol. Phys.* **1997**, *90*, 415.

(71) Boublík, T. *Mol. Phys.* **1989**, *68*, 191.

(72) Rowlinson, J. S.; Swinton, F. L. *Liquids and Liquid Mixtures*, 3rd ed.; Butterworth Scientific: London, 1982.

(73) Boublík, T. *J. Chem. Phys.* **1970**, *53*, 471.

(74) Mansoori, G. A.; Carnahan, N. F.; Starling, K. E.; Leland, T. W. *J. Chem. Phys.* **1971**, *54*, 1523.

(75) Scott, R. L.; van Konynenburg, P. H. *Discuss. Faraday Soc.* **1970**, *49*, 87. van Konynenburg, P. H.; Scott, R. L. *Philos. Trans. R. Soc. London, A.* **1980**, *298*, 495.

(76) Press, W. H.; Teukolsky, S. A.; Vetterling, W. T.; Flannery, B. P. *Numerical Recipes in Fortran*, 1st ed.; Cambridge University Press: 1986.

(77) *Handbook of Chemistry and Physics*, 60th ed.; CRC Press: Boca Raton, FL, 1981.

(78) Physical Property Data, KLEA 32, ICI Chemicals and Polymers Ltd., 1993. Physical Property Data, KLEA 134a, ICI Chemicals and Polymers Ltd., 1993.

(79) Vieweg, R. *Chem. Tech. (Leipzig)* **1963**, *15*, 734.

(80) Lee, J.; Kim, H.; Lim, J. S.; Kim, J.-D.; Lee, Y. Y. *J. Chem. Eng. Data* **1996**, *41*, 43.

(81) Wilson, H. L.; Wilding, W. V. *DIPPRE Data Ser.* **1994**, *2*, 63.